International Journal of Bifurcation and Chaos, Vol. 14, No. 7 (2004) 2513–2524

SIMPLE CHAOTIC CIRCUIT USING CMOS RING OSCILLATORS

YASUTERU HOSOKAWA
Department of Information Science, Shikoku University, Tokushima 771-1192, Japan
hosokawa@keiei.shikoku-u.ac.jp

YOSHIFUMI NISHIO
Department of Electrical and Electronic Engineering, Tokushima University, Tokushima 770-8506, Japan
nishio@ee.tokushima-u.ac.jp

Received January 14, 2003; Revised August 18, 2003

In this study, a chaotic circuit suitable for an integrated circuit is proposed. The circuit consists of two CMOS ring oscillators and a pair of diodes. By using a simplified model of the circuit, the mechanism of generating chaos is explained and the exact solutions are derived. The exact expressions of the Poincaré map and its Jacobian matrix make those possible to confirm the generation of chaos using the Lyapunov exponents and to investigate the related bifurcation phenomena.

Keywords: Chaotic circuit; CMOS; ring oscillator; Lyapunov exponents.

1. Introduction

There are several possibilities of engineering applications with chaos, and they have been investigated by many researchers passionately in the past 10 years. For realizing such applications, an integration of chaotic circuits is a very important subject. The advantages of an integrated circuit are power saving and miniaturization of circuits. Further, in the case of chaos synchronization being utilized in the application, less parameter errors of circuit elements are needed. By fabricating several identical chaotic circuits on the same silicon chip, the resulting circuits are almost the same [Lozi & Chua, 1993]. This becomes more important if a large number of chaotic cells are needed to exploit several features of chaotic networks.

On the other hand, various chaotic circuits have been realized as integrated circuits [Cruz & Chua, 1992; Kanou *et al.*, 1993; Rodríguez-Vázquez, 1998; Eguchi *et al.*, 1998]. However, because the purpose of these studies was to realize Chua's circuit on the IC, the realized circuits have relatively complex structures, which need high integration techniques. The goal of our study is to integrate a chaotic circuit having a simple structure and a small size. One of the attractions of chaos has been that simple systems generate complex phenomena. We go back again to this attraction, namely we try to propose a simple integrated circuit generating chaos.

In this study, we propose a simple chaotic circuit suitable for integration. At first, we take note of a CMOS ring oscillator, which is one of the simplest functional circuits constructed on the chip. The oscillator consists of the odd number of CMOS inverters and is used for a CMOS process performance test. Our chaotic circuit is based on two CMOS ring oscillators and a pair of diodes. Therefore, we consider that the proposed circuit is

realized on the chip very easily. By SPICE simulations of the circuit, we can observe that the periodic orbit bifurcates to chaos via torus. In order to analyze these phenomena in detail, we derive a simplified model of the circuit. The simplified model consists of some linear functions and one piecewise-linear function. The model reveals the physical mechanism of the generation of chaos. Further, the exact solutions can be derived from the model. The exact expressions of the Poincaré map and its Jacobian matrix make those possible to confirm the generation of chaos using the Lyapunov exponents and to investigate the related bifurcation phenomena.

2. Design of Chaotic Circuit

Figure 1 shows a three-stage ring oscillator. This oscillator consists of three CMOS inverters. In the case of the CMOS performance test, many odd number of inverters are coupled and the performance is given as an oscillation frequency. Figure 2 shows SPICE simulation results of the ring oscillator in Fig. 1. Channel width of p-MOS is 60 μm and length is 4 μm and channel width of n-MOS is 20 μm and length is 4 μm, $V_{dd} = 2.70$ V and $V_{ss} = 2.30$ V. These parameters and other SPICE parameters are chosen by taking into account an implementation with 0.5 μm CMOS integrated circuit technology.

We design a chaotic circuit using the ring oscillators as shown in Fig. 3. In order to control amplitudes of oscillators, R_1 and R_2 are connected. The frequency of the upper side oscillator is controlled by C_1. Figure 4 shows SPICE simulation results of the chaotic circuit in Fig. 3. Channel width of p-MOS is 60 μm and length is 4 μm and channel width of n-MOS is 20 μm and length is 4 μm. $V_{dd} = 2.70$ V, $V_{ss} = 2.30$ V, $R_1 = 3000\ \Omega$ and

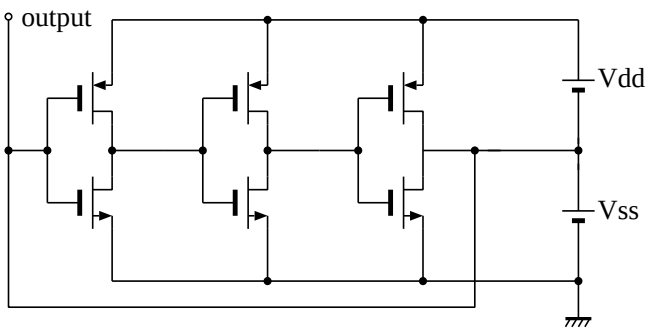

Fig. 1. Three-stage ring oscillator.

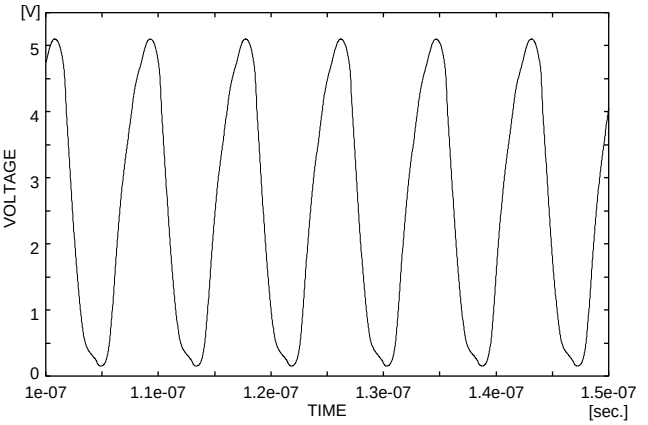

Fig. 2. SPICE simulation result of the ring oscillator in Fig. 1. Channel width of p-MOS is 60 μm and length is 4 μm and channel width of n-MOS is 20 μm and length is 4 μm. $V_{dd} = 2.70$ V and $V_{ss} = 2.30$ V. Maximum time step is 50 ps and analysis time is 10–100 μs.

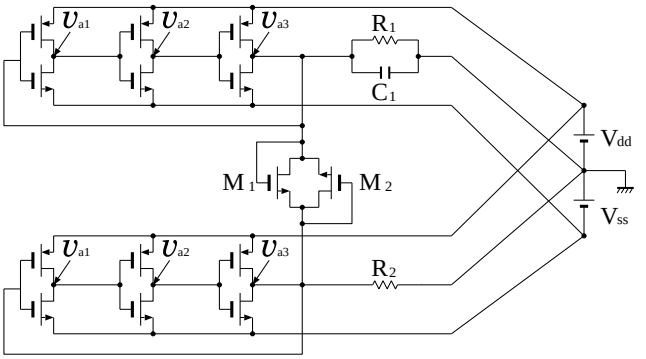

Fig. 3. Chaotic circuit.

$C_1 = 9.00$ pF. We can observe that a periodic orbit (a) bifurcates to torus (b) and (c) and chaos (d) and (e). The main oscillation frequency bandwidth is about 100–250 MHz. Additionally, we have confirmed numerically that all inverters utilize their linear regions only.

Remark. In our early study, we have proposed a design methodology of chaotic circuits [Hosokawa & Nishio, 2002], namely connecting two oscillatory elements by a nonlinear resistor. The present circuit is designed according to this methodology. We consider that the result of this study supports the effectiveness of the methodology.

3. Simplified Model of Chaotic Circuit

In order to analyze the phenomena observed from the SPICE simulations, a simplified model of the

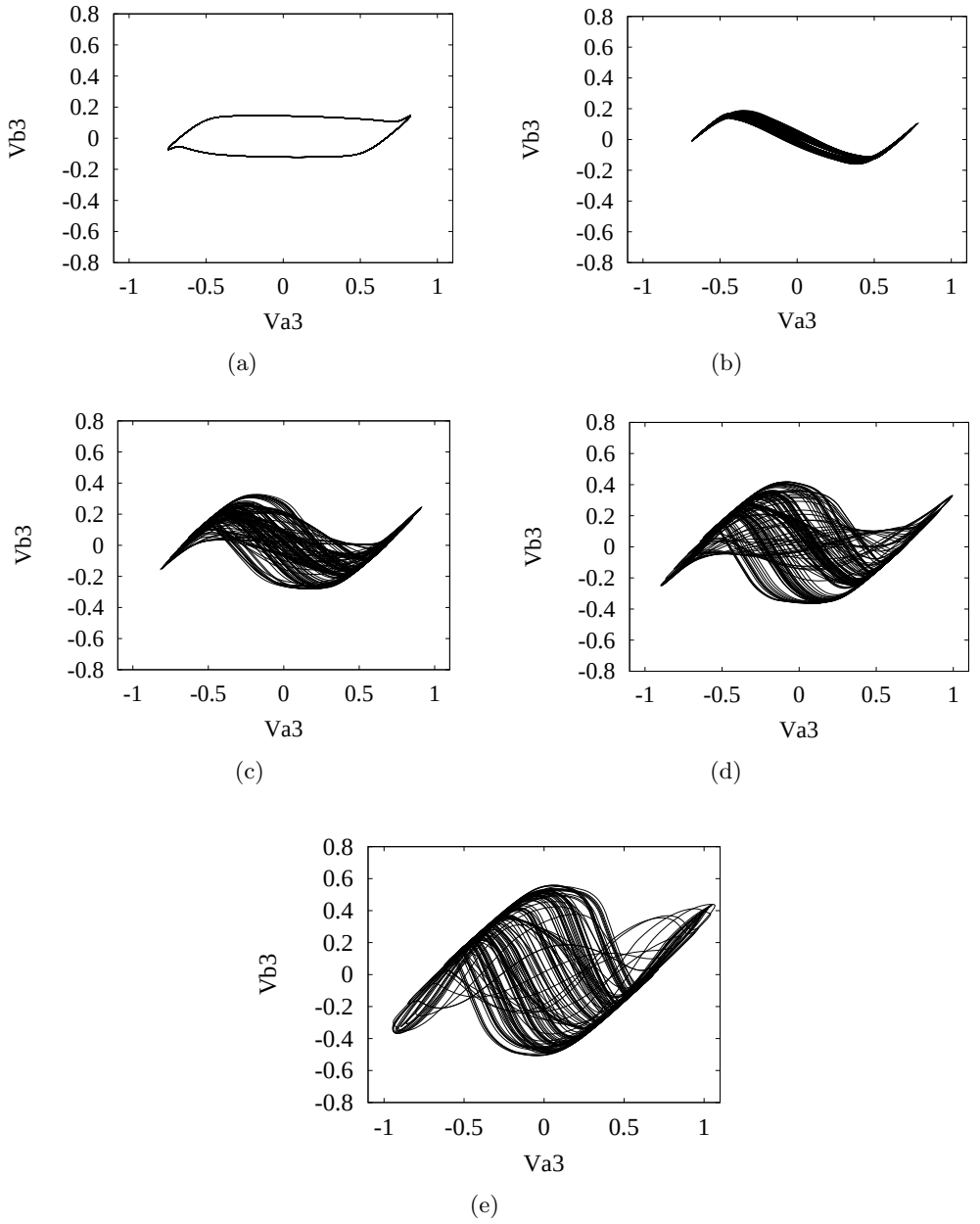

Fig. 4. SPICE simulation result of the chaotic circuit in Fig. 3. Channel width of p-MOS is 60 μm and length is 4 μm and channel width of n-MOS is 20 μm and length is 4 μm. $V_{dd} = 2.70$ V, $V_{ss} = 2.30$ V, $R_1 = 3000\ \Omega$ and $C_1 = 9.00$ nF. (a) $R_2 = 50.0\ \Omega$. (b) $R_2 = 100.0\ \Omega$. (c) $R_2 = 125.0\ \Omega$. (d) $R_2 = 150.0\ \Omega$. (e) $R_2 = 200.0\ \Omega$.

chaotic circuit is derived as two three-dimensional autonomous oscillatory circuits coupled by a pair of diodes.

Figure 5 shows how to derive a simplified model of the inverter in the ring oscillators. Exploiting the fact that all inverters operate only in their linear regions, they can be assumed to be linear elements including voltage controlled current sources. Now, we focus our attention on one inverter. All parasitic capacitors associated with the input node are connected parallel with all parasitic capacitors associated with the output node of the previous stage inverter. The input resistor is connected parallel with the output resistor of the previous stage inverter. Therefore, we can obtain the simplified inverter model as shown at the bottom in Fig. 5.

Since the pair of transistors $M1$ and $M2$ in Fig. 3 has the same characteristics as a pair of diodes shown in Fig. 6(b), we approximate their v–i characteristics by the following three-region

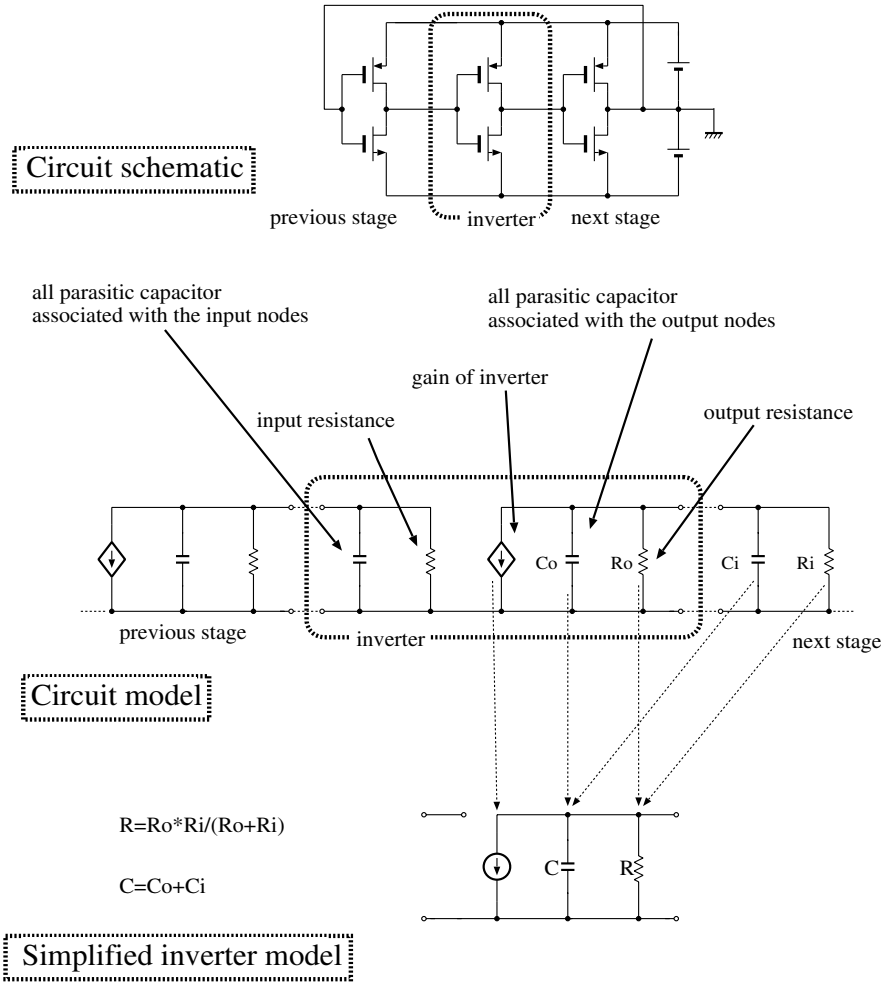

Fig. 5. Deriving simplified inverter model.

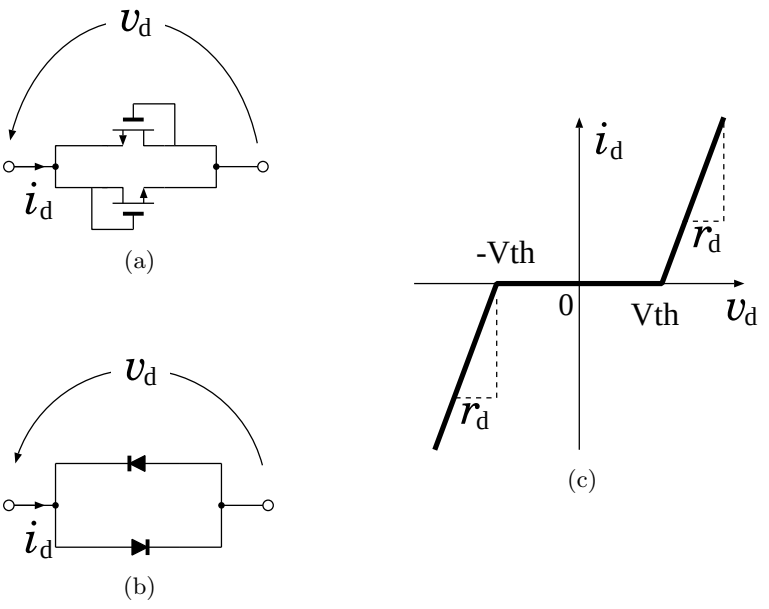

Fig. 6. Pair of transistors and its v–i characteristics.

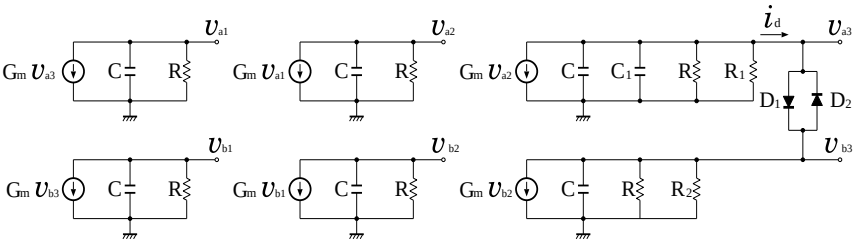

Fig. 7. Simplified model of the chaotic circuit in Fig. 3.

piecewise-linear function as shown in Fig. 6(c).

$$i_d = \begin{cases} \dfrac{1}{r_d}(v_d - V_{th}) & \text{for } v_d > V_{th}\,, \\ 0 & \text{for } |v_d| \le V_{th}\,, \\ \dfrac{1}{r_d}(v_d + V_{th}) & \text{for } v_d < -V_{th}\,. \end{cases} \tag{1}$$

By using the inverter model in Fig. 5 and the pair of diodes in Fig. 6, the simplified model can be shown as Fig. 7. The circuit equations of the simplified model are described as follows:

$$\begin{cases} \dfrac{dv_{a1}}{dt} = -\dfrac{1}{RC}\,v_{a1} - \dfrac{G_m}{C}\,v_{a3}\,, \\ \dfrac{dv_{a2}}{dt} = -\dfrac{1}{RC}\,v_{a2} - \dfrac{G_m}{C}\,v_{a1}\,, \\ \dfrac{dv_{a3}}{dt} = -\dfrac{R+R_1}{RR_1(C+C_1)}\,v_{a3} \\ \qquad\quad -\dfrac{G_m}{C+C_1}\,v_{a3} - \dfrac{i_d}{C+C_1}\,, \\ \dfrac{dv_{b1}}{dt} = -\dfrac{1}{RC}\,v_{b1} - \dfrac{G_m}{C}\,v_{b3}\,, \\ \dfrac{dv_{b2}}{dt} = -\dfrac{1}{RC}\,v_{b2} - \dfrac{G_m}{C}\,v_{b1}\,, \\ \dfrac{dv_{b3}}{dt} = -\dfrac{R+R_2}{RR_2C}\,v_{b3} - \dfrac{G_m}{C}\,v_{b3} + \dfrac{i_d}{C}\,, \end{cases} \tag{2}$$

where

$$i_d = \begin{cases} \dfrac{1}{r_d}(v_{a3} - v_{b3} - V_{th}) & \text{for } v_{a3} - v_{b3} > V_{th}\,, \\ 0 & \text{for } |v_{a3} - v_{b3}| \le V_{th}\,, \\ \dfrac{1}{r_d}(v_{a3} - v_{b3} + V_{th}) & \text{for } v_{a3} - v_{b3} < -V_{th}\,. \end{cases} \tag{3}$$

By substituting the normalized variables and the parameters;

$$\begin{gathered} x_{str} = \frac{v_{str}}{V_{th}}\,, \quad y_d = \frac{R_d}{V_{th}} i_d\,, \quad \tau = \frac{1}{RC}\,t\,, \\ \alpha = G_m R\,, \quad \beta = \frac{C}{C+C_1}\,, \quad \gamma = \frac{R}{R_1}\,, \\ \delta = \frac{R}{R_d}\,, \quad \varepsilon = \frac{R}{R_2}\,, \end{gathered} \tag{4}$$

Eqs. (2) and (3) are normalized as

$$\begin{cases} \dot{x}_{a1} = -x_{a1} - \alpha x_{a3}\,, \\ \dot{x}_{a2} = -x_{a2} - \alpha x_{a1}\,, \\ \dot{x}_{a3} = -\beta(\gamma+1)x_{a3} - \alpha\beta x_{a2} - \beta\delta y_d\,, \\ \dot{x}_{b1} = -x_{b1} - \alpha x_{b3}\,, \\ \dot{x}_{b2} = -x_{b2} - \alpha x_{b1}\,, \\ \dot{x}_{b3} = -(\varepsilon+1)x_{b3} - \alpha x_{b2} + \delta y_d\,, \end{cases} \tag{5}$$

where

$$y_d = \begin{cases} x_{a3} - x_{b3} - 1 & \text{for } x_{a3} - x_{b3} > 1\,, \\ 0 & \text{for } |x_{a3} - x_{b3}| \le 1\,, \\ x_{a3} - x_{b3} + 1 & \text{for } x_{a3} - x_{b3} < -1\,. \end{cases} \tag{6}$$

4. Analysis of Simplified Model

Because the simplified model derived in the previous section is piecewise-linear, we can describe the exact expressions of the solutions, the Poincaré map and its Jacobian matrix.

4.1. *Characteristic equations*

We define three piecewise-linear regions as follows.

$$\begin{aligned} \mathbf{R}_+ &\equiv \{(x_{a1}, x_{a2}, x_{a3}, x_{b1}, x_{b2}, x_{b3}) | x_{a3} - x_{b3} > 1\}\,, \\ \mathbf{R_0} &\equiv \{(x_{a1}, x_{a2}, x_{a3}, x_{b1}, x_{b2}, x_{b3}) || x_{a3} - x_{b3}| \le 1\}\,, \\ \mathbf{R}_- &\equiv \{(x_{a1}, x_{a2}, x_{a3}, x_{b1}, x_{b2}, x_{b3}) | x_{a3} - x_{b3} < -1\}\,. \end{aligned} \tag{7}$$

Table 1. Three piecewise-linear regions.

	State of Diodes	
Region	D1	D2
$\mathbf{R}_+$	ON	OFF
$\mathbf{R_0}$	OFF	OFF
$\mathbf{R}_-$	OFF	ON

These regions correspond to the three different states of the diodes as Table 1. Note that the circuit equations in $\mathbf{R_0}$ are completely decoupled into two three-dimensional equations, because $y_d = 0$. Let us consider eigenvalues in the three regions of the circuit equations in order to derive exact solutions. The characteristic equation of the circuit equations in each linear region is given as follows:

In $\mathbf{R}_\pm$:

$$\begin{aligned} &m^6 + \{5 + \delta + \beta(1 + \gamma + \delta) + \varepsilon\}m^5 + [10 + 4\delta + 4\varepsilon \\ &\quad + \beta\{5 + \varepsilon + \delta(6 + \varepsilon) + \gamma(5 + \delta + \varepsilon)\}]m^4 \\ &\quad + [\alpha^3(1 + \beta) + 2[5 + 3\delta + 3\varepsilon + \beta\{5 + 7\delta + 2\varepsilon \\ &\quad + 2\delta\varepsilon + \gamma(5 + 2\delta + 2\varepsilon)\}]]m^3 \\ &\quad + [5 + 4\delta + 4\varepsilon + \alpha^3\{2 + \beta(4 + \gamma + 2\delta + \varepsilon)\} \\ &\quad + 2\beta\{5 + 8\delta + 3\varepsilon + 3\delta\varepsilon + \gamma(5 + 3\delta + 3\varepsilon)\}]m^2 \\ &\quad + [1 + \delta + \varepsilon + \alpha^3\{1 + \beta(5 + 2\gamma + 4\delta + 2\varepsilon)\} \\ &\quad + \beta\{5 + 9\delta + 4\varepsilon + 4\delta\varepsilon + \gamma(5 + 4\delta + 4\varepsilon)\}]m \\ &\quad + \beta\{1 + \alpha^6 + 2\delta + \varepsilon + \delta\varepsilon + \gamma(1 + \delta + \varepsilon) \\ &\quad + \alpha^3(2 + \gamma + 2\delta + \varepsilon)\} = 0\,. \end{aligned} \tag{8}$$

In $\mathbf{R_0}$:

For upper side circuit,

$$\begin{aligned} &m^3 + \{2 + \beta(\gamma + 1)\}m^2 + \{1 + 2\beta(\gamma + 1)\}m \\ &\quad + \beta(\alpha^3 + \gamma + 1) = 0\,. \end{aligned} \tag{9}$$

For lower side circuit,

$$m^3 + (\varepsilon + 3)m^2 + (2\varepsilon + 3)m + \alpha^3 + \varepsilon + 1 = 0\,. \tag{10}$$

We can calculate the eigenvalues in each region from the characteristic equations (8)–(10).

4.2. *Exact solutions*

We consider the case that the characteristic equation (8) has two real and two pairs of complex conjugate eigenvalues and that (9) and (10) have a real and a pair of complex conjugate eigenvalues, because chaotic attractors can be observed only for such parameter values. We denote the eigenvalues in each region as follows:

$\mathbf{R}_\pm$: λ_{01}, λ_{02}, $\sigma_{01} \pm j\omega_{01}$, $\sigma_{02} \pm j\omega_{02}$,

$\mathbf{R_0}$ (upper side circuit): λ_{11}, $\sigma_{11} \pm j\omega_{11}$,

$\mathbf{R_0}$ (lower side circuit): λ_{12}, $\sigma_{12} \pm j\omega_{12}$.

Further, we define the equilibrium points in $\mathbf{R}_\pm$ as

$$\begin{aligned} &\pm\mathbf{E_e} = \\ &[\pm E_{a1} \quad \pm E_{a2} \quad \pm E_{a3} \quad \pm E_{b1} \quad \pm E_{b2} \quad \pm E_{b3}]^T\,. \end{aligned} \tag{11}$$

These values are calculated by making the right-hand side of Eq. (5) to be equal to zero. The equilibrium point in $\mathbf{R}_0$ is the origin.

Then, we can describe the exact solutions in each linear region as follows.

In $\mathbf{R}_\pm$:

$$\mathbf{x}(\tau) \mp \mathbf{E_e} = \mathbf{F}(\tau) \cdot \mathbf{F}^{-1}(0) \cdot (\mathbf{x}(0) \mp \mathbf{E_e})\,,$$

where

$$\begin{aligned} \mathbf{x}(\tau) &= [x_{a1}(\tau) \quad x_{a2}(\tau) \quad x_{a3}(\tau) \quad x_{b1}(\tau) \\ &\quad x_{b2}(\tau) \quad x_{b3}(\tau)]^T\,, \\ \mathbf{F}(\tau) &= [\mathbf{f_{a1}}(\tau) \quad \mathbf{f_{a2}}(\tau) \quad \mathbf{f_{a3}}(\tau) \quad \mathbf{f_{b1}}(\tau) \\ &\quad \mathbf{f_{b2}}(\tau) \quad \mathbf{f_{b3}}(\tau)]^T\,, \\ \mathbf{f_{a2}}(\tau) &= [e^{\lambda_{01}\tau} \quad e^{\lambda_{02}\tau} \quad e^{\sigma_{01}\tau}\cos\omega_{01}\tau \\ &\quad e^{\sigma_{01}\tau}\sin\omega_{01}\tau \quad e^{\sigma_{02}\tau}\cos\omega_{02}\tau \\ &\quad e^{\sigma_{02}\tau}\sin\omega_{02}\tau]^T\,, \\ \mathbf{f_{a1}}(\tau) &= -\frac{1}{\alpha}\left(\frac{d\mathbf{f_{a2}}(\tau)}{d\tau} + \mathbf{f_{a2}}(\tau)\right), \\ \mathbf{f_{a3}}(\tau) &= -\frac{1}{\alpha}\left(\frac{d\mathbf{f_{a1}}(\tau)}{d\tau} + \mathbf{f_{a1}}(\tau)\right), \\ \mathbf{f_{b3}}(\tau) &= \frac{1}{\beta\delta}\frac{d\mathbf{f_{a3}}(\tau)}{d\tau} + \frac{\gamma + \delta + 1}{\delta}\,\mathbf{f_{a3}}(\tau) + \frac{\alpha}{\delta}\,\mathbf{f_{a2}}(\tau)\,, \\ \mathbf{f_{b2}}(\tau) &= -\frac{d\mathbf{f_{b3}}(\tau)}{d\tau} - \frac{\delta + \varepsilon + 1}{\alpha}\,\mathbf{f_{b3}}(\tau) + \frac{\delta}{\alpha}\,\mathbf{f_{a3}}(\tau)\,, \\ \mathbf{f_{b1}}(\tau) &= -\frac{1}{\alpha}\left(\frac{d\mathbf{f_{b2}}(\tau)}{d\tau} + \mathbf{f_{b2}}(\tau)\right). \end{aligned} \tag{12}$$

In $\mathbf{R_0}$:

$$\mathbf{x_a}(\tau) = \mathbf{G_a}(\tau) \cdot \mathbf{G_a}^{-1}(0) \cdot \mathbf{x_a}(0)\,,$$
$$\mathbf{x_b}(\tau) = \mathbf{G_b}(\tau) \cdot \mathbf{G_b}^{-1}(0) \cdot \mathbf{x_b}(0)\,,$$

where

$$\mathbf{x_a}(\tau) = [x_{a1}(\tau) \quad x_{a2}(\tau) \quad x_{a3}(\tau)]^T\,,$$
$$\mathbf{x_b}(\tau) = [x_{b1}(\tau) \quad x_{b2}(\tau) \quad x_{b3}(\tau)]^T\,,$$
$$\mathbf{G_a}(\tau) = [\mathbf{g_{a1}}(\tau) \quad \mathbf{g_{a2}}(\tau) \quad \mathbf{g_{a3}}(\tau)]^T\,,$$
$$\mathbf{G_b}(\tau) = [\mathbf{g_{b1}}(\tau) \quad \mathbf{g_{b2}}(\tau) \quad \mathbf{g_{b3}}(\tau)]^T\,,$$
$$\mathbf{g_{a2}}(\tau) = [e^{\lambda_{11}\tau} \quad e^{\sigma_{11}\tau}\cos\omega_{11}\tau \quad e^{\sigma_{11}\tau}\sin\omega_{11}\tau]^T\,,$$
$$\mathbf{g_{b2}}(\tau) = [e^{\lambda_{12}\tau} \quad e^{\sigma_{12}\tau}\cos\omega_{12}\tau \quad e^{\sigma_{12}\tau}\sin\omega_{12}\tau]^T\,,$$
$$\mathbf{g_{a1}}(\tau) = -\frac{1}{\alpha}\left(\frac{d\mathbf{g_{a2}}(\tau)}{d\tau} + \mathbf{g_{a2}}(\tau)\right),$$
$$\mathbf{g_{a3}}(\tau) = -\frac{1}{\alpha}\left(\frac{d\mathbf{g_{a1}}(\tau)}{d\tau} + \mathbf{g_{a1}}(\tau)\right),$$
$$\mathbf{g_{b1}}(\tau) = -\frac{1}{\alpha}\left(\frac{d\mathbf{g_{b2}}(\tau)}{d\tau} + \mathbf{g_{b2}}(\tau)\right),$$
$$\mathbf{g_{b3}}(\tau) = -\frac{1}{\alpha}\left(\frac{d\mathbf{g_{b1}}(\tau)}{d\tau} + \mathbf{g_{b1}}(\tau)\right). \tag{13}$$

4.3. *Poincaré map*

In order to confirm the generation of chaos and to investigate the related bifurcation scenario, we derive the Poincaré map. Let us define the following subspace

$$\mathbf{S} = \mathbf{S_1} \cap \mathbf{S_2} \tag{14}$$

where

$$\begin{aligned}&\mathbf{S_1}\text{: } x_{a3} - x_{b3} = 1\\ &\mathbf{S_2}\text{: } \alpha\beta x_{a2} + \beta(\gamma+1)x_{a3} - \alpha x_{b2}\\ &\qquad -(\varepsilon+1)x_{b3} < 0\,.\end{aligned} \tag{15}$$

The subspace $\mathbf{S_1}$ corresponds to the boundary condition between $\mathbf{R}_+$ and $\mathbf{R_0}$, while the subspace $\mathbf{S_2}$ corresponds to the condition $\dot{x}_{a3} - \dot{x}_{b3} > 0$. Namely, $\mathbf{S}$ corresponds to the transitional condition from $\mathbf{R_0}$ to $\mathbf{R}_+$. Let us consider the solution starting from an initial point on $\mathbf{S}$. The solution returns back to $\mathbf{S}$ again after wandering several subspaces as shown in Fig. 8. Hence, we can derive the Poincaré map as follows:

$$\mathbf{T} : \mathbf{S} \to \mathbf{S}\,, \quad \mathbf{x_0} \mapsto \mathbf{T}(\mathbf{x_0})\,, \tag{16}$$

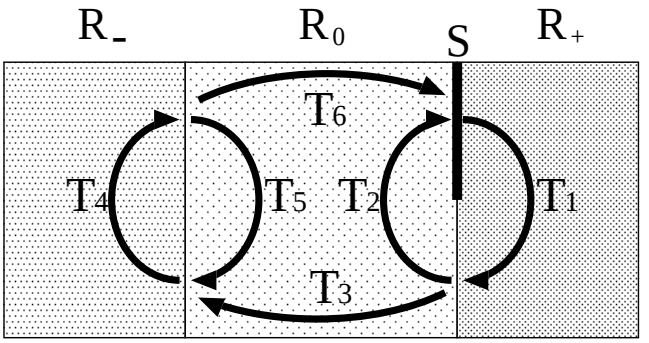

Fig. 8. Route map.

where $\mathbf{x_0}$ is an initial point on $\mathbf{S}$, while $\mathbf{T}(\mathbf{x_0})$ is the point at which the solution starting from $\mathbf{x_0}$ hits $\mathbf{S}$ again. The Poincaré map can be represented as a composite map of the submaps $\mathbf{T_1}$, $\mathbf{T_2} \cdots \mathbf{T_6}$ in Fig. 8, which correspond to the route of the solution.

As an example, let us derive the Poincaré map for the case that the solution starting from $\mathbf{S}$ returns back to $\mathbf{S}$ again via the regions $\mathbf{R}_+$ and $\mathbf{R_0}$. In this case, the Poincaré map can be obtained as

$$\mathbf{T} = \mathbf{T_2} \circ \mathbf{T_1}\,. \tag{17}$$

Each submap can be given as follows. Suppose that the solution starts from

$$\mathbf{x_0} = (X_{a10},\, X_{a20},\, X_{a30},\, X_{b10},\, X_{b20},\, X_{a30} - 1)$$

at $\tau = 0$ and that it hits $\mathbf{S_1}$ and enters $\mathbf{R_0}$ at

$$\mathbf{x_1} = (X_{a11},\, X_{a21},\, X_{a31},\, X_{b11},\, X_{b21},\, X_{a31} - 1)$$

at $\tau = \tau_1$. In this case, $\mathbf{x_1}$ is given by

$$\begin{bmatrix} X_{a11} - E_{a1} \\ X_{a21} - E_{a2} \\ X_{a31} - E_{a3} \\ X_{b11} - E_{b1} \\ X_{b21} - E_{b2} \\ X_{a31} - 1 - E_{b3} \end{bmatrix}$$

$$= \mathbf{F}(\tau_1) \cdot \mathbf{F}^{-1}(0) \cdot \begin{bmatrix} X_{a10} - E_{a1} \\ X_{a20} - E_{a2} \\ X_{a30} - E_{a3} \\ X_{b10} - E_{b1} \\ X_{b20} - E_{b2} \\ X_{a30} - 1 - E_{b3} \end{bmatrix} \tag{18}$$

where τ_1 is obtained by solving the third and sixth rows of Eq. (18). We can calculate the submap

$\mathbf{T_1}$ as

$$\mathbf{x_1} = \mathbf{T_1}(\mathbf{x_0}) \tag{19}$$

Further, suppose that the solution hits $\mathbf{S}$ again at

$$\mathbf{x_2} = (X_{a12},\, X_{a22},\, X_{a32},\, X_{b12},\, X_{b22},\, X_{a32} - 1)$$

at $\tau = \tau_1 + \tau_2$. In this case, $\mathbf{x_2}$ is given by

$$\begin{bmatrix} X_{a12} \\ X_{a22} \\ X_{a32} \end{bmatrix} = \mathbf{G_a}(\tau_2) \cdot \mathbf{G_a^{-1}}(0) \cdot \begin{bmatrix} X_{a11} \\ X_{a21} \\ X_{a31} \end{bmatrix}$$

$$\begin{bmatrix} X_{b12} \\ X_{b22} \\ X_{a32} - 1 \end{bmatrix} = \mathbf{G_b}(\tau_2) \cdot \mathbf{G_b^{-1}}(0) \cdot \begin{bmatrix} X_{b11} \\ X_{b21} \\ X_{a31} - 1 \end{bmatrix} \tag{20}$$

where τ_2 is obtained by solving the third and sixth rows of Eq. (20). We can calculate the submap $\mathbf{T_2}$ as

$$\mathbf{x_2} = \mathbf{T_2}(\mathbf{x_1}) \tag{21}$$

In the same way, we can derive the other composite maps.

4.4. *Lyapunov exponents*

The Jacobian matrix $\mathbf{DT}$ of the Poincaré map can be also derived as a product of the Jacobian matrices of the submaps corresponding to the route of the solution. As an example, we show the Jacobian matrix of the above Poincaré map $\mathbf{T} = \mathbf{T_2} \circ \mathbf{T_1}$.

$$\mathbf{DT} = \mathbf{DT_2} \cdot \mathbf{DT_1}\,. \tag{22}$$

$$\mathbf{DT_1} = \begin{bmatrix} 1 & 0 & \dfrac{X_{a11} + \alpha X_{a31}}{A_1} & 0 & 0 & -\dfrac{X_{a11} + \alpha X_{a31}}{A_1} \\ 0 & 1 & \dfrac{\alpha X_{a11} + X_{a21}}{A_1} & 0 & 0 & -\dfrac{\alpha X_{a11} + X_{a21}}{A_1} \\ 0 & 0 & \dfrac{(\varepsilon+1)X_{a31} + \alpha X_{b21} - \varepsilon - 1}{A_1} & 0 & 0 & \dfrac{\alpha\beta X_{a21} + \beta(\gamma+1)X_{a31}}{A_1} \\ 0 & 0 & \dfrac{\alpha X_{a31} + X_{b11} - \alpha}{A_1} & 0 & 0 & -\dfrac{\alpha X_{a31} + X_{b11} + \alpha}{A_1} \\ 0 & 1 & \dfrac{\alpha X_{b11} + X_{b21}}{A_1} & 0 & 0 & -\dfrac{\alpha X_{b11} + X_{b21}}{A_1} \end{bmatrix} \cdot \mathbf{F}(\tau_1) \cdot \mathbf{F^{-1}}(\mathbf{0}) \cdot \begin{bmatrix} 1 & 0 & 0 & 0 & 0 \\ 0 & 1 & 0 & 0 & 0 \\ 0 & 0 & 1 & 0 & 0 \\ 0 & 0 & 0 & 1 & 0 \\ 0 & 0 & 0 & 0 & 1 \\ 0 & 0 & 1 & 0 & 0 \end{bmatrix} \tag{23}$$

where

$$A_1 = -\alpha\beta X_{a21} + \{-\beta(\gamma+1) + \varepsilon + 1\}X_{a31} + \alpha X_{b21} - \varepsilon - 1\,. \tag{24}$$

$$\mathbf{DT_2} = \begin{bmatrix} 1 & 0 & \dfrac{X_{a12} + \alpha X_{a32}}{A_2} & 0 & 0 & -\dfrac{X_{a12} + \alpha X_{a32}}{A_2} \\ 0 & 1 & \dfrac{\alpha X_{a12} + X_{a22}}{A_2} & 0 & 0 & -\dfrac{\alpha X_{a12} + X_{a22}}{A_2} \\ 0 & 0 & \dfrac{(\varepsilon+1)X_{a32} + \alpha X_{b22} - \varepsilon - 1}{A_2} & 0 & 0 & \dfrac{\alpha\beta X_{a22} + \beta(\gamma+1)X_{a32}}{A_2} \\ 0 & 0 & \dfrac{\alpha X_{a32} + X_{b12} - \alpha}{A_2} & 0 & 0 & -\dfrac{\alpha X_{a32} + X_{b12} - \alpha}{A_2} \\ 0 & 1 & \dfrac{\alpha X_{b12} + X_{b22}}{A_2} & 0 & 0 & -\dfrac{\alpha X_{b12} + X_{b22}}{A_2} \end{bmatrix} \cdot \mathbf{G}(\tau_2) \cdot \mathbf{G^{-1}}(\mathbf{0}) \cdot \begin{bmatrix} 1 & 0 & 0 & 0 & 0 \\ 0 & 1 & 0 & 0 & 0 \\ 0 & 0 & 1 & 0 & 0 \\ 0 & 0 & 0 & 1 & 0 \\ 0 & 0 & 0 & 0 & 1 \\ 0 & 0 & 1 & 0 & 0 \end{bmatrix} \tag{25}$$

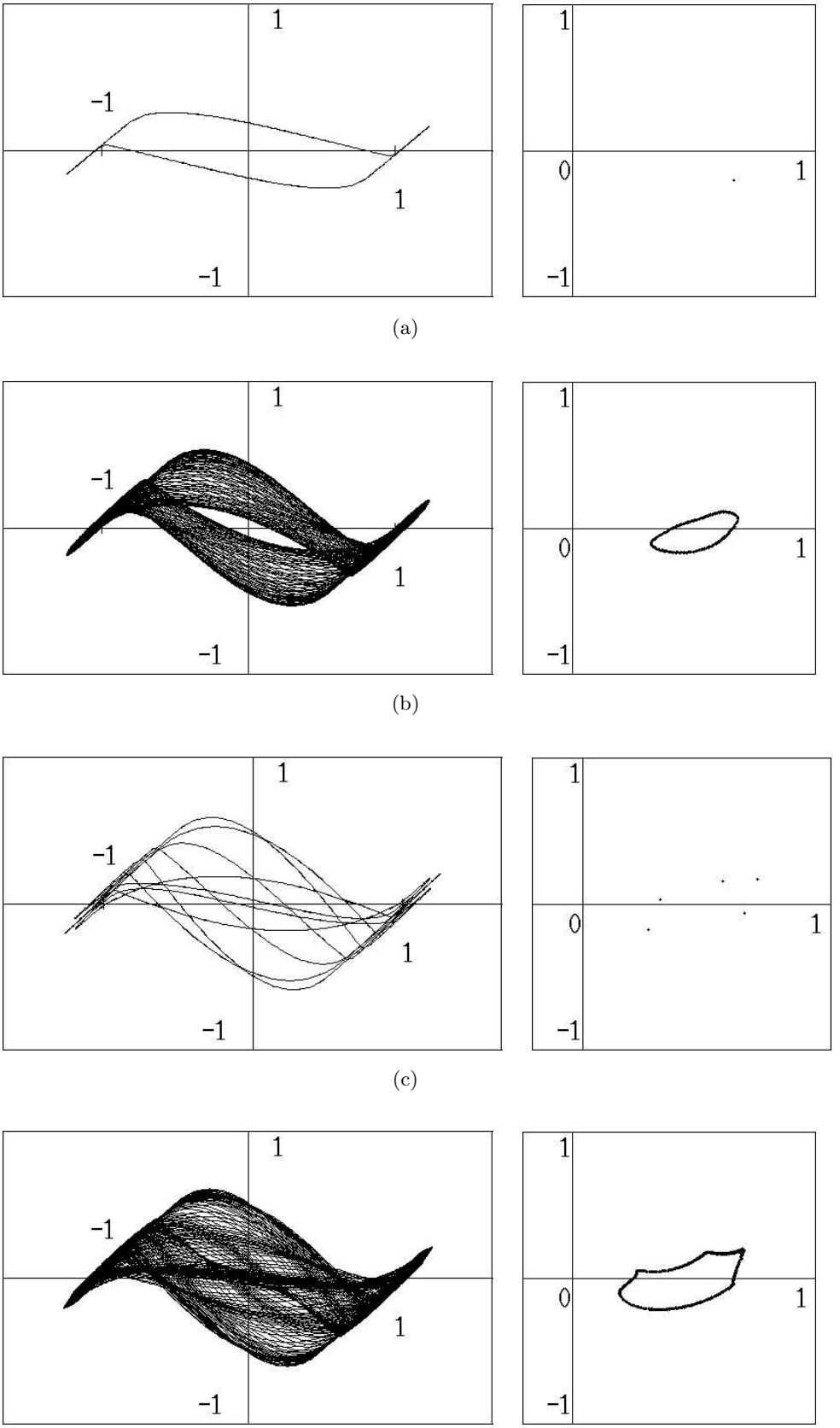

Fig. 9. Projection of attractors onto x_{a3}–x_{b3} plane (left) and their Poincaré maps (right). $\alpha = 4.0$, $\beta = 0.1$, $\gamma = 5.0$ and $\delta = 50$. (a) $\varepsilon = 10.0$. (b) $\varepsilon = 3.30$. (c) $\varepsilon = 3.05$. (d) $\varepsilon = 2.90$. (e) $\varepsilon = 2.75$. (f) $\varepsilon = 2.66$. (g) $\varepsilon = 2.57$. (h) $\varepsilon = 2.40$.

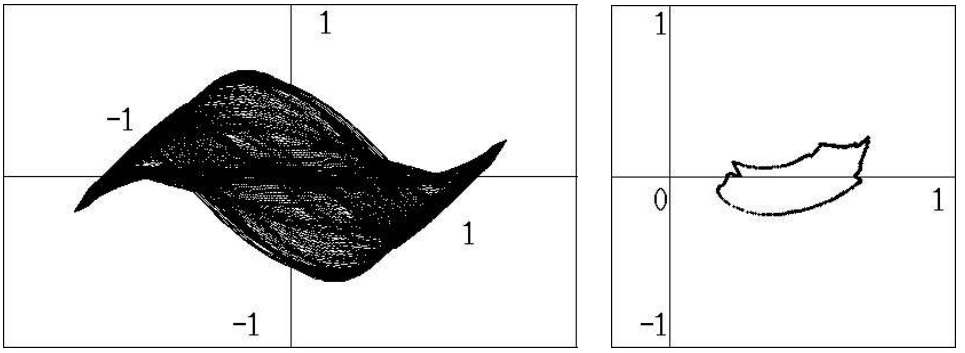

(e)

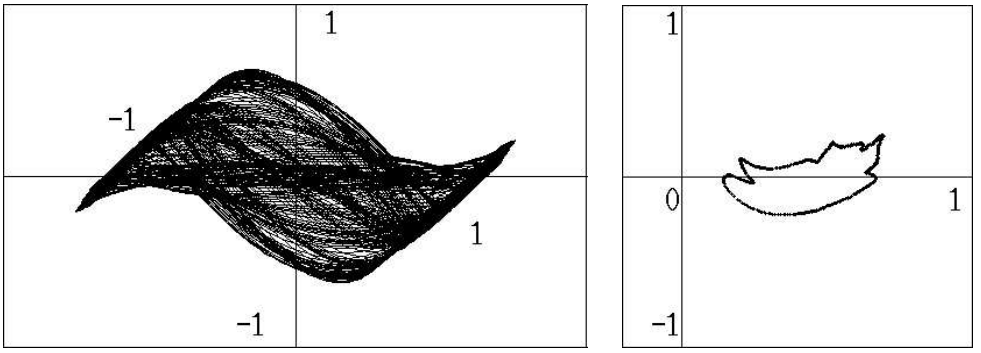

(f)

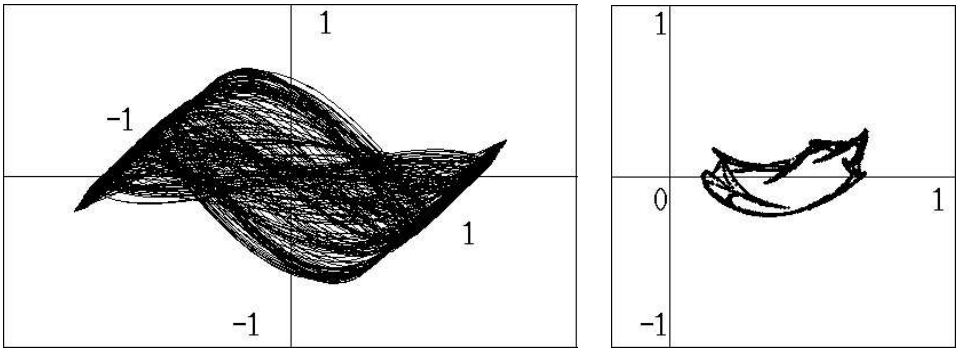

(g)

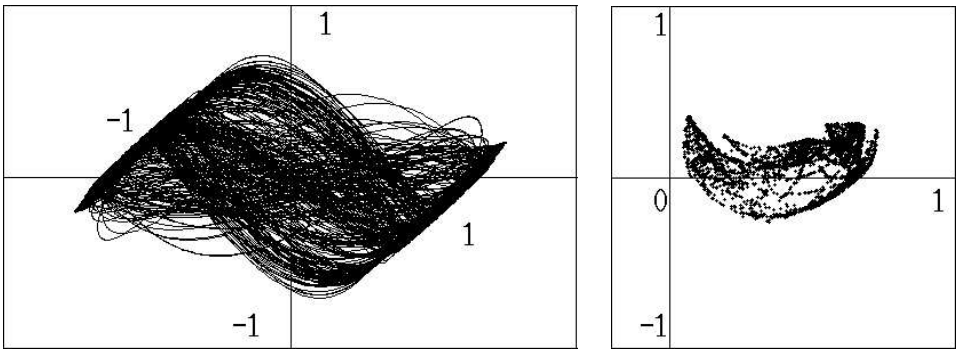

(h)

Fig. 9 (*Continued*)

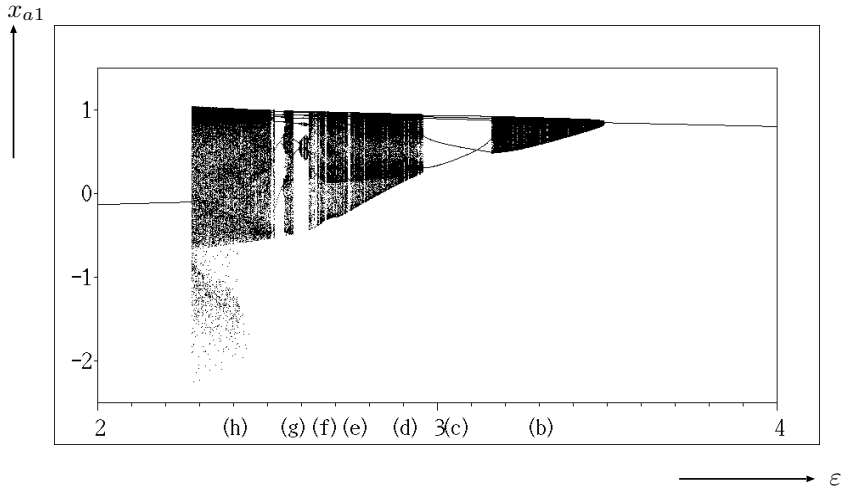

(a)

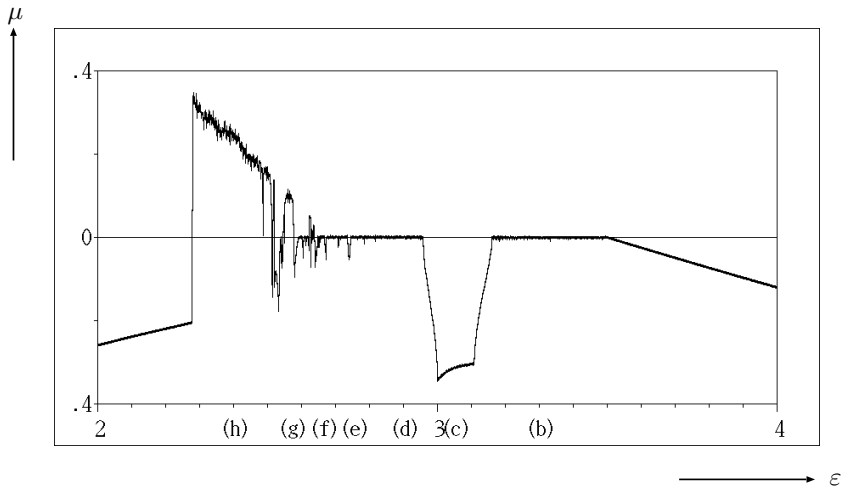

(b)

Fig. 10. (a) One-parameter bifurcation diagram. (b) Largest Lyapunov exponent. $\alpha = 4.0$, $\beta = 0.1$, $\gamma = 5.0$ and $\delta = 50$.

where

$$\mathbf{G}(\tau) = [\mathbf{G_a}(\tau)^T \quad \mathbf{G_b}(\tau)^T]^T \,, \tag{26}$$

$$A_2 = -\alpha\beta X_{a22} + \{-\beta(\gamma+1) + \varepsilon + 1\} X_{a32} + \alpha X_{b22} - \varepsilon - 1 \,. \tag{27}$$

By using the Jacobian Matrix, we can calculate the largest Lyapunov exponent;

$$\mu = \lim_{N\to\infty} \frac{1}{N} \sum_{j=1}^{N} \log |\mathbf{DT}(j) \cdot \mathbf{e}(j)| \tag{28}$$

where $\mathbf{e}(j)$ is a normalized basis.

5. Computer Calculated Results

Figure 9 (left) shows the projections of attractors onto x_{a3}–x_{b3} plane obtained by calculating Eqs. (12) and (13). We can say that these results are similar to the SPICE simulation results in Fig. 4. Namely, the simplified model in Sec. 3 does not lose important features of the original circuit related with the generation of chaotic behavior. This means that the ring oscillators in the original circuit behave as simple divergently oscillating parts, and only the nonlinearity of the pair of diodes controls the amplitude. In other words, the ring oscillators play a role of expanding, while the coupling diodes play a role of folding. These two features, expanding and folding, are known as the essence of generating chaos.

The Poincaré maps are shown in Fig. 9 (right). One-periodic orbit (a) bifurcates to torus (b) around $\varepsilon = 3.50$. Periodic window (c) can be observed in the torus region. As ε decreases, torus grows (d) and starts to break down (e) and (f). From the shape of the Poincaré maps, we can estimate that attractors in (g) and (h) are chaos.

One-parameter bifurcation diagram and the calculated largest Lyapunov exponent are shown in Figs. 10(a) and 10(b), respectively. The control parameter is ε and the other parameters are fixed. As shown in Fig. 10, the Lyapunov exponent takes positive values for a relatively wide range of ε. Hence, the proposed circuit can be said to generate chaos. Moreover, we can describe the detailed bifurcation scenario as follows. For $3.15 < \varepsilon < 3.50$, torus appears. We observed a large number of phase-locked states in this torus region. However, we cannot see the states in the diagram, because the parameter interval corresponding to each phase-locked state is not so large. For $2.95 < \varepsilon < 3.15$, a large window corresponding to the periodic orbit in Fig. 9(c) is observed. For $2.57 < \varepsilon < 2.95$, the largest Lyapunov exponent becomes positive occasionally though the attractor looks like torus. We consider that chaos via folded-torus appears in this interval [Inaba & Mori, 1992]. For $2.57 > \varepsilon$, chaotic attractors can be observed for almost parameter values. We have also confirmed that a lot of small periodic windows are embedded in the chaotic region.

6. Conclusions

In this study, we have proposed a very simple chaotic circuit using CMOS ring oscillators. By using a simplified model, the exact solutions of the circuit were derived. We calculated the Lyapunov exponents and confirmed the generation of chaos. Further, we investigated the related bifurcation phenomena.

The simplified model revealed the physical mechanism of the generation of chaos. Namely, the ring oscillators play a role of expanding and the coupling diodes play a role of folding, which are known as the essence of generating chaos.

Because we chose the circuit parameters and other SPICE parameters as taking into account an implementation with 0.5 μm CMOS integrated circuit technology, we believe that the proposed circuit can be realized on IC chip easily.

References

Cruz, J. M. & Chua, L. O. [1992] "A CMOS IC nonlinear resistor for Chua's circuit," *IEEE Trans. Circuits Syst.-I* **39**, 985–995.

Delgado-Restituto, M. & Rodríguez, A. [1998] "Design considerations for integrated continuous-time chaotic oscillators," *IEEE Trans. Circuits Syst.-I* **45**, 481-495.

Eguchi, K., Inoue, T. & Tsuneda, A. [1998] "FPGA implementation of a digital chaos circuit realizing a 3-dimensional chaos model," *IEICE Trans. Funds.* **E81-A**, 1176–1178.

Hosokawa, Y. & Nishio, Y. [2002] "A design method for chaotic circuits using two oscillators," in *Chaos in Circuits and Systems*, eds. Chen, G. & Ueta, T. (World Scientific, Singapore), Chap. 3, pp. 51–69.

Inaba, N. & Mori, S. [1992] "Folded torus in the forced Rayleigh oscillator with a diode pair," *IEEE Trans. Circuits Syst.-I* **39**, 402–411.

Kanou, N., Horio, Y., Aihara, K. & Nakamura, S. [1993] "A current-mode circuit of a chaotic neuron model," *IEICE Trans. Fund.* **E76-A**, 642–644.

Lozi, R. & Chua, L. O. [1993] "Secure communications via chaotic synchronization II: Noise reduction by cascading two identical receivers," *Int. J. Bifurcation and Chaos* **3**, 1319–1325.